Order to disorder transition due to entropy in layered and 2D carbides

Brian C. Wyatt [1], Yinan Yang [2], Paweł P. Michałowski [3*], Tetiana Parker [4], Yamilée Morency [5], Francesca Urban [4], Givi Kadagishvili [6], Manushree Tanwar [6], Sixbert P. Muhoza [7], Srinivasa Kartik Nemani [8,†], Annabelle Bedford [1], Hui Fang [6], Zachary D. Hood [7], Junwoo Jang [8], Krutarth Kamath [1], Bethany G. Wright [8], Rebecca Disko [8], Anupma Thakur [1], Sanguk Han [5], Neil Ghosh [8], Xianfan Xu [8], Zahra Fakhraai [6*], Yury Gogotsi [4*], Aleksandra Vojvodic [5*], De-en Jiang [2*], Babak Anasori [1,8*]

[1]School of Materials Engineering, Purdue University, West Lafayette, IN 47907, USA
[2]Department of Chemical and Biomolecular Engineering, Vanderbilt University, Nashville, TN 37235, USA
[3]Łukasiewicz Research Network - Institute of Microelectronics and Photonics, Warsaw, Poland
[4]A.J. Drexel Nanomaterials Institute and Department of Materials Science and Engineering, Drexel University, Philadelphia, PA 19104, USA
[5]Department of Chemical and Biomolecular Engineering, University of Pennsylvania, Philadelphia, Pennsylvania 19104, USA
[6]Department of Chemistry, University of Pennsylvania, Philadelphia, PA 19104, USA
[7]Applied Materials Division, Argonne National Laboratory, Lemont, IL 60439, USA
[8]School of Mechanical Engineering, Purdue University, West Lafayette IN 47907, USA

[†] Present address at Department of Mechanical and Materials Engineering, University of Alabama Birmingham, Birmingham, AL 35294, USA

*Corresponding authors. Email: banasori@purdue.edu, de-en.jiang@vanderbilt.edu, alevoj@seas.upenn.edu, gogotsi@drexel.edu, fakhraai@sas.upenn.edu, pawel.michalowski@imif.lukasiewicz.gov.pl

Abstract:

In compositionally complex materials, there is controversy on the effect of enthalpy versus entropy on the structure and short-range ordering in so-called high-entropy materials. To help address this controversy, we synthesized and probed 40 M_4AlC_3 layered carbide phases containing 2 to 9 metals and found that short-range ordering from enthalpy is present until the entropy increases enough to achieve complete disordering of the transition metals in their atomic planes. We transformed all these layered carbide phases into two-dimensional (2D) sheets and showed the effects of the order vs. disorder on their surface properties and electronic behavior. This study suggests the key effect that the competition between enthalpy and entropy has on short-range order in multi-compositional materials.

Main text:

Alloys containing stoichiometric mixtures of metallic elements in high-entropy alloys were systematically explored in the early 2000s (*1, 2*) which demonstrated increased mechanical properties (*3*) and decreased thermal conductivity (*4*) beyond normal expectations of the "rule of mixture" approximations (*3-7*). In one of the early studies (*1*), it was proposed that increasing the total number of metallic elements in a single-phase material could result in entropy-stabilization of enthalpically unfavorable mixtures of elements, which gained this class of metals the descriptor "high-entropy" alloys. Since this early report, high-entropy materials have been reported in other metallic alloys (*8*) as well as carbides (*9*), oxides (*10*), diborides (*11*), and other ceramics (*12*). However, since the "high-entropy" descriptor became popular, there has been pushback to using it as a general label (*13*), as it may not fully represent the major effect that enthalpy still has on the stability of a single-phase system. For example, short-range ordering in some high-entropy systems (*14-17*) suggests that enthalpic effects must still be present, even in entropy-stabilized materials (*18*). Therefore, there is a basic need to evaluate the true role of entropy vs. enthalpy in the achieved configurations in single-phase "high-entropy" materials.

MAX phases are chemically denoted by their formula $M_{n+1}AX_n$, where M refers to $n+1$ layers of one or more early transition metals that are interleaved by X, which represents n layers of carbon/nitrogen (*19*). Between these $M_{n+1}X_n$ slabs, there are monoatomic layers of one or more A elements (commonly from groups 13-16 of the periodic table) (*20*). M is ionic/covalently bonded to X (*21*), similar to a transition metal carbide (*22*), while the surface M of each $M_{n+1}X_n$ slab is metallically bonded to the A element (*21*), which is structurally similar to a stacking fault in layered ceramics (*23, 24*). As a result of this different structure and bonding at the $M_{n+1}X_n$-A-$M_{n+1}X_n$ interface, there can be a preference for the ordering of two or more transition metals in separate transition metal planes (*25*). When n is more than 1 in $M_{n+1}AX_n$, some transition metals prefer M sites bonded to both X and to A (M′ layers) or M sites only bonded to X (M″ layers), which is referred to as o-MAX (Figure 1A for M = 2) (*26-28*).

Although these o-MAX phases were reported a decade ago in two transition metal systems (*29*), the preference for an M′ vs. an M″ site in MAX phases is not fully understood. Computationally, it has been shown that Group 6 transition metals, such as Cr, Mo, and W prefer M′ sites while Group 4 transition metals, such as Ti, Zr, and Hf prefer M″ sites (*30, 31*). Similarly, the earliest reported "high-entropy" 2D MXenes, in 2021, $(TiVCrMo)_4C_3$ and $(TiVNbMo)_4C_3$ (*32*), were still predicted to have Cr and Mo in M′ sites and Ti and Nb in M″ sites (*33*). As MXenes are derived from their precursor MAX phases (*34*), this suggests that even in entropy-stabilized MAX phases (*32*), the enthalpic preference of M′ or M″ site occupancy is likely present.

We report the synthesis of 40 compositionally complex MAX phases containing 2 to 9 transition metals. We demonstrate that MAX and MXenes let us evaluate the short-range ordering in multi-elemental materials and demonstrate the effects of enthalpy vs. entropy on the order-to-disorder transition at the smallest scale (i.e., a few layers of atoms).

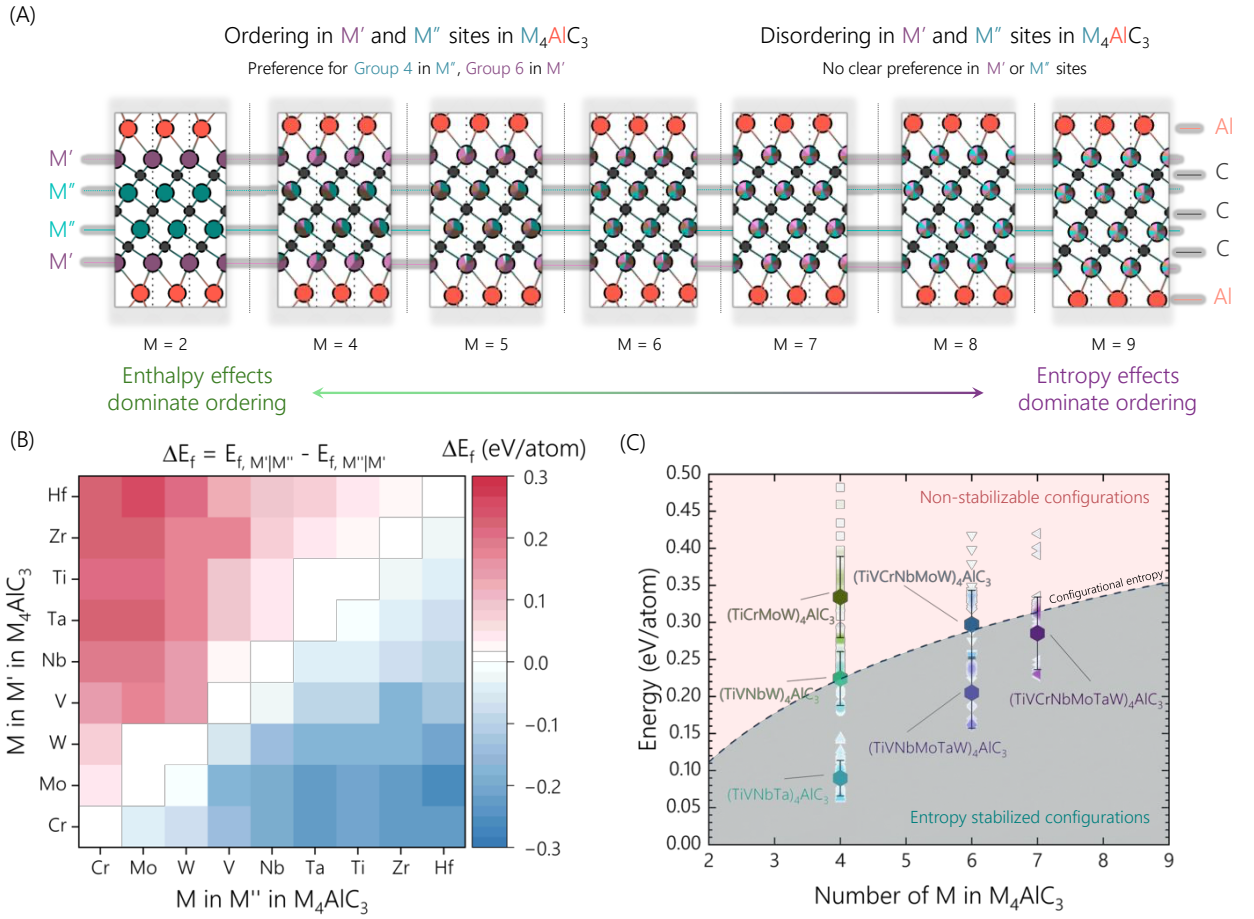

Fig. 1. Enthalpy vs. entropy competition toward order-disorder in M_4AlC_3 MAX phases. (A) Schematic showing the hypothesis of increasing disorder with increasing entropy in M_4AlC_3 MAX phases. **(B)** The difference in formation energies for different pairs of transition metals in either M' or M'' sites in M_4AlC_3 MAX. **(C)** Formation energy above the hull (ΔE_{hull}) vs. configurational entropy in M_4AlC_3 MAX phases with the formation energy vs. entropy-crossover around 7 transition metals. Error bars represent standard deviation.

Theoretical studies of the order-to-disorder transition

To gain insight into the competition between enthalpy and entropy toward the order-disorder transition in high-entropy MAX phases (Figure 1A), we first used density functional theory (DFT). To understand the M′ vs. M″ preference for different transition metals in the M_4AlC_3 MAX phase, we built a symmetric model considering a pair (M_1 and M_2) of transition metals in either M′ or M″ layers (M_1-C-M_2-C-M_2-C-M_1) for all the possible combinations (from 2 to 9 elements) (Figure S1). Figure S2 shows the formation energy (E_f) of these configurations; the calculation details are reported in the supporting information (Methods & Table S1-S3).

After calculating these formation energies, we next used the difference in the formation energy (ΔE_f) between these structures with two given transition metals in either M′ and M″ sites to observe the enthalpic preference of the transition metals to different layers in the M_4C_3 structure (Figure 1B). We focused on identifying the preference for an out-of-plane ordering for an M (i.e.,

to order in separate transition metal planes), which we found has a higher effect on the formation energy than any in-plane order (Figures S3-S5). Trend-wise, we observed that the M′ preference is Cr > Mo > W > V > Nb > Ta > Ti > Zr > Hf (inverse for M″ preference). This trend agrees with previous studies on both binary and high-entropy MAX phase (and carbide) literature, which show that Group 6 transition metals are usually less stable in the M_6C octahedra and, in MAX, tend to segregate toward M sites closest to the A layer (*9, 30*). Overall, we show this preference is still present in M_4AlC_3 structures with >2 transition metals.

We used our model for short-range order to evaluate this hypothesis, given the clear preference for transition metal arrangement in the M_4AlC_3 MAX phase structure. We first analyzed the M_4AlC_3 MAX phase structures with 4 transition metals: $(TiVNbTa)_4AlC_3$, $(TiVNbW)_4AlC_3$, and $(TiCrMoW)_4AlC_3$. Broadly, we find that when the same preference for order as found in double transition metal o-MAX (labeled "ordered") is matched (Figures S4-S6), the lowest formation energies are achieved. For example, when V and W occupy only M′ (outer) sites and Ti and Nb occupy only M″ (inner) sites in $(TiVNbW)_4AlC_3$, the formation energy is -0.544 ± 0.001 eV/atom. In contrast, if Ti and Nb occupy only M′ sites and V and W occupy only M″ sites, opposite the previous reports of o-MAX phases (labeled "inverse ordered"), the formation energy is -0.430 ± 0.001 eV/atom. Similarly, solid solution occupancies of Ti and Nb in M′ and M″ sites have a higher formation energy of -0.485 ± 0.006 eV/atom for $(TiVNbW)_4AlC_3$ than the ordered configuration.

Additionally, we found that group 6 elements always increased the distribution of the energy penalty, as it is energetically preferred for group 6 elements to be in the M′ over M″ sites (Figure S6). Broadly, this suggests two things: 1) MAX phases containing group 6 elements are generally less energetically favored, and 2) group 6 elements, if present, will most likely be in the M′ site. However, we found that the formation energy of MAX phases containing group 6 elements decreased with the increasing number of transition metals, which provides an avenue to their inclusion in MAX and potential MXenes (Figure S6). Therefore, based on analyzing the contributions of enthalpy and entropy across several compositions (Figures S5, S6), we predict that the transition from order to disorder likely occurs when a seventh element is introduced. However, due to the extensive computational demand, it was not feasible in the present study to simulate all possible compositions. A summary of this analysis of formation energy vs. configurational entropy for the MAX phases containing 4, 6, and 7 transition metals is shown in Figure 1C, where the configurations below the dotted line are stabilizable by entropy and the configurations above the dotted line are not stabilizable by entropy.

Experimental observation of the order-to-disorder transition due to entropy

With the gained knowledge from the energetic perspective, we next experimentally synthesized M_4AlC_3 MAX phases containing combinations of 2 and 4 to 9 elements of Group 4, 5, and 6 transition metals (Figure 2A-B). Synthesis and other details for these phases are in the supporting information. To see if we experimentally observed ordering in M_4AlC_3 MAX phases, we first analyzed the x-ray diffraction (XRD) patterns (Figures S7-S8). All of the 40 phases

reported in this work can be found in Table S4. All MAX phase characterization and analysis for each phase reported can be found in Figures S9-S44. Figure 2C shows the scanning electron microscopy (SEM) image of $(TiVCrZrNbMoHfTaW)_4AlC_3$ with a layered grain structure; the energy dispersive X-ray spectroscopy (EDS) shows that the grain contains all 9 transition metals as well as Al (Figure 2D). The XRD data (Figures S9-S44) shows the presence of impurity phases, including intermetallics and non-MAX carbides, which suggests that subsequent studies are required to improve the phase purity of these MAX phases. Although the XRD data provides some insight into the ordering, it is difficult to accurately compare transition metals with very similar X-ray scattering features (i.e., Ti vs. V or Cr, Zr vs. Nb or Mo, Hf vs. Ta or W) even when using Rietveld refinement. Therefore, we used an atomic-layer resolved dynamic secondary ion mass spectrometry (SIMS) method, as this method is better suited for differentiating the transition metals by elemental mass and charge (*35-37*).

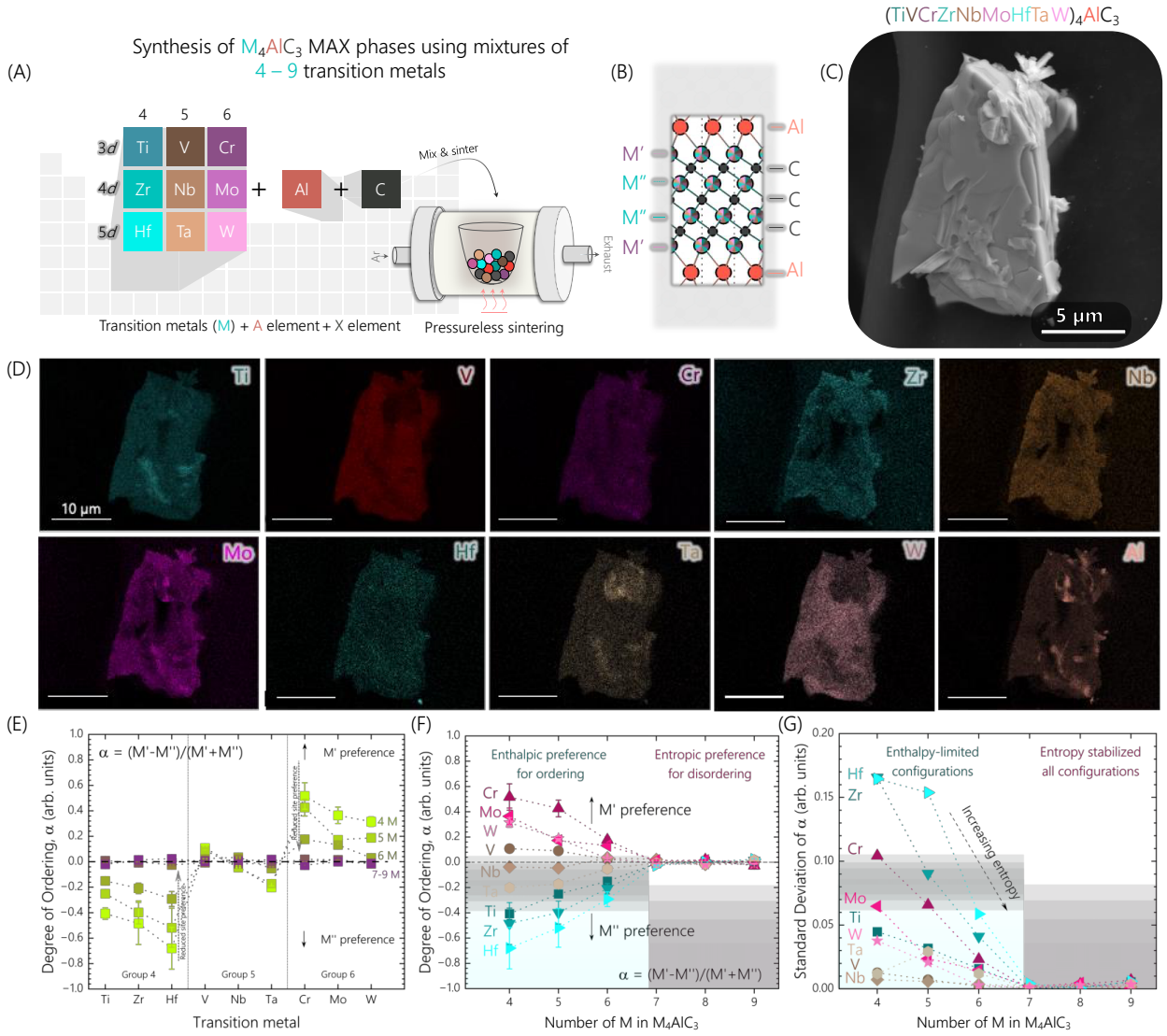

Fig. 2. Synthesis and analysis of $(TiVCrZrNbMoHfTaW)_4AlC_3$ and other M_4AlC_3 phases containing 2 to 9 transition metals. (A) Schematic highlighting the mixed elements and synthesis approach. **(B)** Crystal structure of the targeted M_4AlC_3 MAX phase. **(C)** Electron microscopy image of a grain of $(TiVCrZrNbMoHfTaW)_4AlC_3$ MAX.

(D) Elemental mapping of a grain of $(TiVCrZrNbMoHfTaW)_4AlC_3$ MAX showing the presence of all 9 transition metals and aluminum. **(E)** Secondary ion mass spectrometry (SIMS) measurements show the preference for sites based on the transition metal and the total number of transition metals in M_4AlC_3 MAX. **(F)** SIMS shows the decreasing preference for different sites in M_4AlC_3 MAX plotted against the increasing numbers of transition metals. **(G)** Decrease in standard deviation in the ordering term a as calculated by SIMS plotted against the increasing numbers of transition metals. All error bars represent standard deviation.

To calculate the preference for site occupancy using SIMS, we determined atomic composition from the signal intensity (*37*) and calculated the average and standard deviation the occupancy of each element in either the M′ or M″ site. We then calculated a unitless comparative parameter, labeled α, for each transition metal from these values using Eq. 1 (*33*). As a result, when α is positive, it represents that a given transition metal prefers the M′ site. The inverse is also true. All standard deviations from the atomic composition were then propagated to this α using the root mean square method.

$$\alpha = \frac{M' - M''}{M' + M''} \qquad \text{Eq. 1}$$

SIMS indicates that Mo always occupies the M′ site and Ti, V, and Nb always occupy the M″ site for M_4AlC_3 MAX phases with two transition metals (Figure S45). This agrees with Figure 1C, which states that Group 6 transition metals most likely occupy M′ sites while Group 4 or 5 occupy M″ sites. Further, to calculate this site preference for M_4AlC_3 MAX phases with 4 or more transition metals, the difference in the atomic composition of each element in the M′ and M″ sites was evaluated by the "α" parameter (Eq. 1). Using this parameter, we noted that when 4 transition metals were placed into the M_4AlC_3 MAX phase, the trend in preference of a transition metal for an M′ or M″ site was the same as established for M_4AlC_3 MAX with two transition metals (Cr > Mo > W > V > Nb > Ta > Ti > Zr > Hf in M′ site) (Figure 2E). This agrees with Figure 1B-C, suggesting that an enthalpic preference for M′ or M″ site ordering of the transition metals is still present even for these entropy-stabilized M_4AlC_3 MAX phases (*32*).

We observed that increasing the number of transition metals to 5 and 6 resulted in a diminished |α| for each transition metal (Figure 2F). Together with Figure 1C, this suggests that configurations with less preference for order are more likely to be stabilized by the increasing configurational entropy. For the SIMS data, this would result in a lower |α| for each transition metal, as ordered (following Figure 1B), and disordered configurations of the transition metals would become observable in each transition metal layer. Probabilistically, however, we would not expect |α| to converge on zero yet in these low-to-medium entropy systems, as inverse-ordered configurations would not yet become stabilizable through entropy.

Conversely, beyond 7 transition metals, we observe that the |α| converges on 0 for all transition metals (Figure 2F). The convergence of |α| to zero suggests that ordered, solid solution, and inverse ordered configurations are stabilized. This would likely result in equal probabilistic chances to observe any configuration via SIMS measurements. We see further support for this

hypothesis by plotting the standard deviation of $|\alpha|$ for all transition metals against the total number of transition metals (Figure 2F), which further suggests that all configurations become stabilized at ≥7 transition metals. Overall, our computational and experimental results indicate that the loss of short-range ordering in high-entropy MAX phases is only achievable once entropy can overcome the enthalpic penalties for all configurations. Broadly, this data demonstrates that (i) entropy-stabilized systems can display a preference for short-range ordering, but (ii) systems only truly become "high-entropy" materials once entropy overcomes any remaining enthalpic preferences for the short-range order. However, high-throughput methods should be implemented to screen the effects of electronegativity, atomic size, electronic structure, oxygen substitution in the X sublattice, and other key features of the ordering and order-to-disorder transition to fully understand this transition. Further, subsequent studies must consider the impact of intermediate phases on the final phase formation and ordering. In addition, while computational studies have shown that out-of-plane ordering trends are similar between $M_{n+1}AX_n$ phases with $n > 2$, subsequent studies should evaluate whether an order-to-disorder transitions are observed in other multi-transition metal MAX phases.

Effect of order vs. disorder on MXenes surface chemistry

After confirming the synthesis and ordering behavior of the M_4C_3 structure in the M_4AlC_3 MAX phases, we evaluated the effect of order vs. disorder and composition on the individual M_4C_3 lamellas. To do so, we synthesized the $M_4C_3T_x$ MXenes from their M_4AlC_3 MAX phases using wet chemical synthesis (Figure 3A) (*28, 31, 32, 34*), which causes the MXene surface to be terminated with T_x groups, commonly -O, -(OH), and -F (*34*). Some XRD patterns of MAX to MXene synthesis are shown in Figure S46. Further, we confirmed that our MXenes contained the same transition metals as the MAX, as shown for $(TiVCrZrNbMoHfTaW)_4C_3T_x$ in Figures S47-S48. In addition, we confirmed using SIMS for some select compositions that the ordering of the transition metals remained similar in the MXenes as it was in the MAX (Figures S49-S52). We also confirmed that we were able to successfully synthesize MXene films for a total number of transition metals between 4 and 9 as shown via XRD in Figure S53. Although we used a similar etching procedure for all MAX phases to obtain MXenes, subsequent studies are necessary to understand the exfoliation energy of each MAX to MXenes to best tune the synthesis process for any individual composition (*38*). All 2D MXenes produced in this study were dispersible in water (Figure S54), however, using X-ray photoelectron spectroscopy (XPS), we observed that the overall composition of T_x in the $M_4C_3T_x$ MXenes containing 4 to 9 transition metals increased for -O (~33 at% to ~53 at%) and decreased for -OH (~37 at% to ~26 at%) and -F (~30 at% to 21 at%) (Figures S55-S63 & Table S5).

The ordering/disordering observed in the MAX phases is present in the MXenes (*36*) (Figures S49-S52) and is a likely source of the changes in the T_x group composition in the respective $M_4C_3T_x$ MXenes. To gain insight into this trend, we used DFT to calculate the formation energy of -O and -F terminations on MXenes with different pairs of transition metals in either M′

or M″ sites (Figure 3B). We observed that pairs of Group 4 elements prefer F terminations, and pairs of Group 6 elements prefer O terminations. We also observed that Group 6 in M″ causes an increased preference for Group 4 in M′ for O terminations, and Group 4 in M″ causes an increased preference for Group 6 in M′ for F terminations. As shown in the supporting information (Figure S64), the solid solution combinations are typically between the two ordered configurations. The calculated values of O vs. F preference for both ordered and solid solution configurations of the paired transition metals are shown in Figure S65.

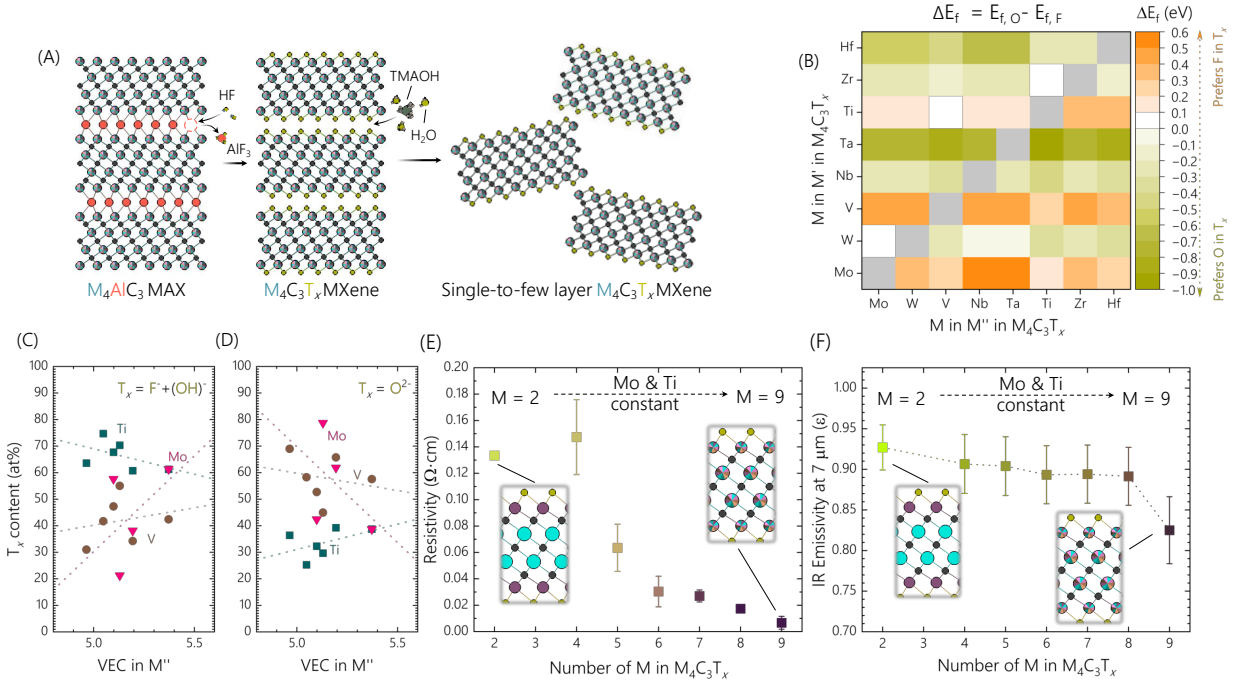

Fig. 3. Synthesis, surface chemistry, and properties of $M_4C_3T_x$ MXenes containing 2 to 9 transition metals. (A) Schematic of the synthesis process of $M_4C_3T_x$ MXenes from M_4AlC_3 MAX. **(B)** Differences in formation energy of pairs of transition metals in $M_4C_3T_x$ with O vs. F in T_x. The greyed boxes represent values that have yet to be calculated. **(C-D)** Content of O and F terminations, respectively, on Ti, V, and Mo atoms in $M_4C_3T_x$ MXenes vs. the valence electrons concentration (VEC) in the M" layers. The dotted lines are guides for the eye. **(E)** Electrical resistivity behavior of $M_4C_3T_x$ MXenes containing 2 to 9 transition metals. **(F)** IR emissivity at 7 mm wavelength plotted against the total number of transition metals in the $M_4C_3T_x$ MXenes. All error bars represent experimental uncertainty.

As we cannot know the exact subsurface M″ metal atom for any given M′ metal atom bonded to T_x in our MXenes, we chose to plot the surface chemistry for M in M′ sites (bonded to T_x) against the valence electron concentration (VEC) in the M″ sites (Figure 3C-D), which was derived from SIMS using formal charges of the transition metals (Ti has 4, V has 5, Cr has 6, *etc.*). In addition, in this plot, we consider both –(OH) and –F terminations together and –O terminations separate, as –(OH) and –F would prefer a T^{-} oxidation state while –O would prefer a T^{2-} oxidation state. We chose to add –(OH) and –F together as our use of tetramethylammonium hydroxide as a delamination agent could replace –F groups with –(OH) groups, and the two share a formal charge. As shown in Figure 3C-D, increasing the VEC in the M″ sites can increase the concentration of O terminations on Ti and –(OH)/F on V and Mo, which is broadly in agreement with the trends shown

in Figure 3B. A plot for easier comparison can be found in Figure S66. We see agreement with the general increase of O as a T_x group on $M_4C_3T_x$ MXenes containing 4 to 9 transition metals (Fourier-transform infrared spectra in Figure S67). In addition, through ultra-violet-visible-near infrared (UV-vis-NIR) and Raman spectroscopy, we gained some insight into the effect of disorder in $M_4C_3T_x$ MXenes by increasing the total number of transition metals (Figures S68-S71). Overall, this suggests surface vs. subsurface transition metals impact the chemical behavior and preference for surface terminations of the MXenes (*39*).

Effect of order vs. disorder on MXenes electrical conductivity

We evaluated the effect of multiple transition metals and order vs. disorder on the electrical properties of thin films of these $M_4C_3T_x$ MXenes. When we investigated the $M_4C_3T_x$ MXenes containing 2 to 9 transition metals, we found that the MXenes retain their metallic conductivity by both their linear *I* vs. *V* behavior as well as their consistency with the Drude model of metallic electrical conductivity (Figures S72-S78) (*40*). In addition, we noted that MXenes that contained Cr were up to an order of magnitude higher in electrical resistivity (Figure S79), which is reported for high-entropy alloys with Cr (*41*). The flake sizes are shown using dynamic light scattering measurements in Figure S80. In Figures S81-S89, atomic force microscopy images, height, and surface roughness analysis of some of the $M_4C_3T_x$ flakes containing 2 – 9 transition metals are shown (Table S6 summarizes the height and surface roughness results).

A decreasing electrical resistivity has been reported for high-entropy alloys with increasing numbers of transition metals (*42*). However, the cause is not yet fully understood. In M_2C-type MXenes, computational work has shown Group 5 transition metals in MXenes should lower the electrical resistivity (*43*) while Group 6 transition metals MXenes have a higher electrical resistivity (*44*). Overall, in our high-entropy $M_4C_3T_x$ MXenes, we expect an increasing number of transition metals to cause disorder of Group 5 and 6 transition metals throughout the $M_4C_3T_x$ structure. Therefore, we first plotted the electrical resistivity of our $M_4C_3T_x$ MXenes against the total number of transition metals, as shown in Figure 3E. In Figure 3E, we chose to keep Ti and Mo as consistent transition metals and systematically add one transition metal at a time to maintain comparability between samples. For example, at M = 2, we show the fully ordered $Mo_2Ti_2C_3T_x$, at M = 4 we show the low entropy $(TiVNbMo)_4C_3T_x$, and then add W, Ta, Cr, Zr, and Hf for M = 5, 6, 7, 8, and 9, respectively.

In Figure 3E, the resistivity of $Mo_2Ti_2C_3T_x$ at 0.13 Ω·cm initially increases for $(TiVNbMo)_4C_3T_x$ to 0.15 ± 0.03 Ω·cm, and then decreases to 0.01 ± 0.01 Ω·cm $(TiVCrZrNbMoHfTaW)_4C_3T_x$. In addition, we observed a similar behavior in the infrared (IR) emissivity of these MXenes (Figure 3F). This agrees with the changes in electrical resistivity shown in Figure 3E, as decreasing electrical resistivity typically will result in a proportional decrease in IR emissivity (*45*). Broadly, we hypothesize that this decrease in resistivity could be attributed to two reasons (Figure S90): 1) the decrease in ordering results in fewer neighbors of Group 6 to Group 6 transition metals, or 2) the decrease in order creates structures with smaller

differences in the total number of valence electrons (averaging to 5) between neighbors in both M′ and M″ layers, both of which could improve the electron mobility in and between the M′ and M″ layers. However, subsequent studies are necessary to better understand the electron mobility and other properties in high-entropy MXenes and other high-entropy materials (*46*), such as approaches that focus on single-flake measurements or optical conductivity (Figure S91).

In summary, this work demonstrates a broad advancement in the understanding of the relation of enthalpy and entropy on short-range ordering in high-entropy materials. Specifically, by using M_4AlC_3 MAX phases with 2 to 9 transition metals and analyzing their structural ordering using SIMS, we were able to evaluate the trend in the short-range ordering of transition metals in either outer (M′) or inner (M″) metal sites against the total number of transition metals. Doing so, we have shown that 1) in low and medium entropy combinations (up to 6 metals), the transition metals enthalpically prefer order in M′ or M″ sites, 2) at 7 metals or above, the structures become fully disordered (no clear preference for M′ or M″), and that this order-disorder transition was 3) driven by an increasing contribution of configurational entropy. Lastly, we showed that these MAX phases can be used to synthesize their respective MXenes, which allowed us to observe some effects of entropically driven disorder in these phases on the electrical and IR emissivity properties of the derived MXenes.

References and Notes

1. J. W. Yeh *et al.*, Nanostructured high-entropy alloys with multiple principal elements: novel alloy design concepts and outcomes. *Advanced Engineering Materials* **6**, 299-303 (2004).
2. B. Cantor, I. Chang, P. Knight, A. Vincent, Microstructural development in equiatomic multicomponent alloys. *Materials Science and Engineering: A* **375**, 213-218 (2004).
3. D. Utt *et al.*, The origin of jerky dislocation motion in high-entropy alloys. *Nature Communications* **13**, 4777 (2022).
4. H.-P. Chou, Y.-S. Chang, S.-K. Chen, J.-W. Yeh, Microstructure, thermophysical and electrical properties in AlxCoCrFeNi (0≤ x≤ 2) high-entropy alloys. *Materials Science and Engineering: B* **163**, 184-189 (2009).
5. L. Han *et al.*, Multifunctional high-entropy materials. *Nature Reviews Materials* **9**, 846-865 (2024).
6. S. Schweidler *et al.*, High-entropy materials for energy and electronic applications. *Nature Reviews Materials* **9**, 266-281 (2024).
7. Y. Zhang, T. Zuo, Y. Cheng, P. K. Liaw, High-entropy alloys with high saturation magnetization, electrical resistivity and malleability. *Scientific Reports* **3**, 1455 (2013).
8. F. Otto, Y. Yang, H. Bei, E. P. George, Relative effects of enthalpy and entropy on the phase stability of equiatomic high-entropy alloys. *Acta Materialia* **61**, 2628-2638 (2013).
9. P. Sarker *et al.*, High-entropy high-hardness metal carbides discovered by entropy descriptors. *Nature Communications* **9**, 4980 (2018).
10. C. M. Rost *et al.*, Entropy-stabilized oxides. *Nature Communications* **6**, 8485 (2015).
11. J. Gild *et al.*, High-entropy metal diborides: a new class of high-entropy materials and a new type of ultrahigh temperature ceramics. *Scientific Reports* **6**, 37946 (2016).
12. C. Oses, C. Toher, S. Curtarolo, High-entropy ceramics. *Nat. Rev. Mater.* **5**, 295-309 (2020).
13. M. Brahlek *et al.*, What is in a name: Defining “high entropy” oxides. *APL Materials* **10**, (2022).
14. S. Chen *et al.*, Simultaneously enhancing the ultimate strength and ductility of high-entropy alloys via short-range ordering. *Nature Communications* **12**, 4953 (2021).
15. P. Singh, A. V. Smirnov, D. D. Johnson, Atomic short-range order and incipient long-range order in high-entropy alloys. *Physical Review B* **91**, 224204 (2015).
16. A. J. Wright, J. Luo, A step forward from high-entropy ceramics to compositionally complex ceramics: a new perspective. *Journal of Materials Science* **55**, 9812-9827 (2020).
17. B. Jiang *et al.*, Probing the local site disorder and distortion in pyrochlore high-entropy oxides. *Journal of the American Chemical Society* **143**, 4193-4204 (2020).
18. S. Divilov *et al.*, Disordered enthalpy–entropy descriptor for high-entropy ceramics discovery. *Nature* **625**, 66-73 (2024).

19. M. Dahlqvist, M. W. Barsoum, J. Rosen, MAX phases–Past, present, and future. *Materials Today* **72**, 1-24 (2024).
20. M. Sokol, V. Natu, S. Kota, M. W. Barsoum, On the Chemical Diversity of the MAX Phases. *Trends in Chemistry* **1**, 210-223 (2019).
21. M. Magnuson, M. Mattesini, Chemical bonding and electronic-structure in MAX phases as viewed by X-ray spectroscopy and density functional theory. *Thin Solid Films* **621**, 108-130 (2017).
22. B. C. Wyatt, S. K. Nemani, G. E. Hilmas, E. J. Opila, B. Anasori, Ultra-high temperature ceramics for extreme environments. *Nature Reviews Materials*, 1-17 (2023).
23. A. Gusev, A. Kurlov, V. Lipatnikov, Atomic and vacancy ordering in carbide ζ-Ta4C3− x (0.28⩽ x⩽ 0.40) and phase equilibria in the Ta–C system. *Journal of Solid State Chemistry* **180**, 3234-3246 (2007).
24. C. R. Weinberger, G. B. Thompson, Review of phase stability in the group IVB and VB transition-metal carbides. *J. Am. Ceram. Soc.* **101**, 4401-4424 (2018).
25. M. Dahlqvist, J. Rosen, The rise of MAX phase alloys–large-scale theoretical screening for the prediction of chemical order and disorder. *Nanoscale* **14**, 10958-10971 (2022).
26. W. Hong, B. C. Wyatt, S. K. Nemani, B. Anasori, Double transition-metal MXenes: Atomistic design of two-dimensional carbides and nitrides. *MRS Bulletin* **45**, 850-861 (2020).
27. B. Anasori *et al.*, Experimental and theoretical characterization of ordered MAX phases Mo_2TiAlC_2 and $Mo_2Ti_2AlC_3$. *Journal of Applied Physics* **118**, (2015).
28. B. C. Wyatt *et al.*, Design of Atomic Ordering in $Mo_2Nb_2C_3T_x$ MXenes for Hydrogen Evolution Electrocatalysis. *Nano Letters*, (2023).
29. Z. Liu *et al.*, (Cr 2/3 Ti 1/3) 3 AlC 2 and (Cr 5/8 Ti 3/8) 4 AlC 3: New MAX-phase Compounds in Ti–Cr–Al–C System. *Journal of the American Ceramic Society* **97**, 67-69 (2014).
30. M. Dahlqvist, J. Rosen, Predictive theoretical screening of phase stability for chemical order and disorder in quaternary 312 and 413 MAX phases. *Nanoscale* **12**, 785-794 (2020).
31. B. Anasori *et al.*, Two-Dimensional, Ordered, Double Transition Metals Carbides (MXenes). *ACS Nano* **9**, 9507-9516 (2015).
32. S. K. Nemani *et al.*, High-Entropy 2D Carbide MXenes: $TiVNbMoC_3$ and $TiVCrMoC_3$. *ACS Nano* **15**, 12815-12825 (2021).
33. Z. Leong *et al.*, Elucidating the chemical order and disorder in high-entropy MXenes: A high-throughput survey of the atomic configurations in TiVNbMoC3 and TiVCrMoC3. *Chemistry of Materials* **34**, 9062-9071 (2022).
34. K. R. G. Lim *et al.*, Fundamentals of MXene synthesis. *Nature Synthesis* **1**, 601–614 (2022).
35. P. P. Michałowski *et al.*, Oxycarbide MXenes and MAX phases identification using monoatomic layer-by-layer analysis with ultralow-energy secondary-ion mass spectrometry. *Nature Nanotechnology* **17**, 1192-1197 (2022).

36. B. C. Wyatt *et al.*, Alkali cation stabilization of defects in 2D MXenes at ambient and elevated temperatures. *Nature Communications* **15**, 6353 (2024).
37. P. P. Michałowski, Unraveling the composition of each atomic layer in the MXene/MAX phase structure–identification of oxycarbide, oxynitride, and oxycarbonitride subfamilies of MXenes. *Nanoscale Horizons* **9**, 1493-1497 (2024).
38. R. Khaledialidusti, M. Khazaei, S. Khazaei, K. Ohno, High-throughput computational discovery of ternary-layered MAX phases and prediction of their exfoliation for formation of 2D MXenes. *Nanoscale* **13**, 7294-7307 (2021).
39. Y. Yang *et al.*, Distinguishing electronic contributions of surface and sub-surface transition metal atoms in Ti-based MXenes. *2D Materials* **7**, (2020).
40. M. Han *et al.*, Beyond $Ti_3C_2T_x$: MXenes for Electromagnetic Interference Shielding. *ACS Nano* **14**, 5008-5016 (2020).
41. K. Jin *et al.*, Tailoring the physical properties of Ni-based single-phase equiatomic alloys by modifying the chemical complexity. *Scientific Reports* **6**, 20159 (2016).
42. S. K. Dewangan, C. Nagarjuna, V. Kumar, in *High Entropy Materials*. (CRC Press), pp. 91-106.
43. M. Han *et al.*, Tailoring Electronic and Optical Properties of MXenes through Forming Solid Solutions. *Journal of the American Chemical Society* **142**, 19110–19118 (2020).
44. M. Khazaei, M. Arai, T. Sasaki, M. Estili, Y. Sakka, Two-dimensional molybdenum carbides: potential thermoelectric materials of the MXene family. *Physical Chemistry Chemical Physics* **16**, 7841-7849 (2014).
45. M. Han *et al.*, Versatility of infrared properties of MXenes. *Materials Today* **64**, 31-39 (2023).
46. Y. Jien-Wei, Recent progress in high entropy alloys. *Ann. Chim. Sci. Mat* **31**, 633-648 (2006).
47. A. Lipatov *et al.*, Electrical and Elastic Properties of Individual Single-Layer $Nb_4C_3T_x$ MXene Flakes. *Advanced Electronic Materials* **6**, (2020).
48. A. Lipatov *et al.*, Effect of synthesis on quality, electronic properties and environmental stability of individual monolayer Ti3C2 MXene flakes. *Advanced Electronic Materials* **2**, 1600255 (2016).
49. J. Halim, K. M. Cook, P. Eklund, J. Rosen, M. W. Barsoum, XPS of cold pressed multilayered and freestanding delaminated 2D thin films of Mo2TiC2Tz and Mo2Ti2C3Tz (MXenes). *Applied Surface Science* **494**, 1138-1147 (2019).
50. J. Halim *et al.*, X-ray photoelectron spectroscopy of select multi-layered transition metal carbides (MXenes). *Applied Surface Science* **362**, 406-417 (2016).
51. R. Simpson, R. G. White, J. F. Watts, M. A. Baker, XPS investigation of monatomic and cluster argon ion sputtering of tantalum pentoxide. *Applied Surface Science* **405**, 79-87 (2017).
52. Z. Yang *et al.*, XPS studies of nitrogen doping niobium used for accelerator applications. *Applied Surface Science* **439**, 1119-1126 (2018).
53. P. Pyykko, M. Atsumi, Molecular single-bond covalent radii for elements 1-118. *Chemistry* **15**, 186-197 (2009).

54. K. Shevchuk, A. Sarycheva, C. E. Shuck, Y. Gogotsi, Raman spectroscopy characterization of 2D carbide and carbonitride MXenes. *Chemistry of Materials* **35**, 8239-8247 (2023).
55. H. Yang, J. Zhang, J. Li, Q. Shen, L. Zhang, In situ preparation and corrosion resistance of a ZrO2 film on a ZrB2 ceramic. *Coatings* **9**, 455 (2019).
56. R. Gautam, S. Vanga, F. Ariese, S. Umapathy, Review of multidimensional data processing approaches for Raman and infrared spectroscopy. *EPJ Techniques and Instrumentation* **2**, 1-38 (2015).
57. D. R. Neuville *et al.*, in *Fiberglass Science and Technology: Chemistry, Characterization, Processing, Modeling, Application, and Sustainability*. (Springer, 2021), pp. 89-216.
58. B. Cantor, Local Nanostructure in Multicomponent High-Entropy Materials. *High Entropy Alloys & Materials*, 1-30 (2024).
59. J. Mendialdua, R. Casanova, Y. Barbaux, XPS studies of V2O5, V6O13, VO2 and V2O3. *Journal of Electron Spectroscopy and Related Phenomena* **71**, 249-261 (1995).
60. D. Pinto *et al.*, Synthesis and electrochemical properties of 2D molybdenum vanadium carbides – solid solution MXenes. *Journal of Materials Chemistry A* **8**, 8957-8968 (2020).
61. K. H. Liland, A. Kohler, N. K. Afseth, Model-based pre-processing in Raman spectroscopy of biological samples. *Journal of Raman Spectroscopy* **47**, 643-650 (2016).
62. Z. Wang *et al.*, Spin-dependent Transport Properties of CrO 2 Micro Rod. *Nano-Micro Letters* **6**, 365-371 (2014).
63. Z. Luo *et al.*, Measurement of in-plane thermal conductivity of ultrathin films using micro-Raman spectroscopy. *Nanoscale and Microscale Thermophysical Engineering* **18**, 183-193 (2014).
64. F. Ding *et al.*, Tailoring planar strain for robust structural stability in high-entropy layered sodium oxide cathode materials. *Nature Energy*, 1-11 (2024).
65. P. P. Michałowski *et al.*, Oxycarbide MXenes and MAX phases identification using monoatomic layer-by-layer analysis with ultralow-energy secondary-ion mass spectrometry. *Nature Nanotechnology* **17**, 1192-1197 (2022).
66. J. Chastain, R. C. King Jr, Handbook of X-ray photoelectron spectroscopy. *Perkin-Elmer Corporation* **40**, 221 (1992).
67. C. Martin *et al.*, Tungsten oxide thin film bombarded with a low energy He ion beam: evidence for a reduced erosion and W enrichment. *Physica Scripta* **2017**, 014019 (2017).
68. H. Fang *et al.*, Stabilizing Ti3C2T x MXene flakes in air by removing confined water. *Proceedings of the National Academy of Sciences* **121**, e2400084121 (2024).
69. W. Ma *et al.*, A novel high-entropy MXene Ti1. 1V1. 2Cr0. 8Nb1. 0Mo0. 9C4Tx for high-performance supercapacitor. *Scripta Materialia* **235**, 115596 (2023).

Acknowledgments: GK and ZF would like to thank Professor Thomas E. Mallouk of the University of Pennsylvania for giving us access to the UV-Vis-NIR spectrometer and the Harrick Plasma Cleaner. GK and ZF would like to thank Richard Stephens for providing valuable ideas.

Funding: National Science Foundation Center for Chemical Innovation (NSF CCI) program grant 2318105 (BCW, YY, TP, YM, FU, GK, MT, SKN, AB, HF, KK, BGW, RD, AT, SS, ZF, YG, AV, DJ, and BA). National Science Foundation Solid State & Materials Chemistry (NSF SSMC) program grant 2419026 (BCW, SKN, AB, KK, BGW, RD, AT, and BA). National Science Centre, Poland, within SONATA BIS 14 2024/54/E/ST11/00171 and the National Centre for Research and Development, Poland, within LIDER XII LIDER/8/0055/L-12/20/NCBR/2021 projects (PPM). Laboratory Directed Research and Development (LDRD) of Argonne National Laboratory, Office of Science, U.S. Department of Energy (DOE), Contract No. DE-AC02-06CH11357 (SPM and ZDH). National Science Foundation Grant CBET-2051525 (JJ, NG, XX). Vagelos Institute for Energy Science and Technology (University of Pennsylvania) graduate fellowship (YM). National Energy Research Scientific Computing Center, a DOE Office of Science User Facility supported by the Office of Science of the U.S. Department of Energy Contract No. DE-AC02-05CH11231 using NERSC award BES-ERCAP0023161 (YM and AV). Ministry of Trade, Industry, and Energy (MOTIE), Korea, under the "Global Industrial Technology Cooperation Center program" (Grant: P0028332) supervised by the Korea Institute for Advancement of Technology (BCW, YG, BA). National Science Foundation Major Research Instrumentation Program (Awards 1229514 and 1429241 to the Integrated Nanosystems Development Institute of Indiana University Indianapolis) (BCW and BA).

Author contributions:

Conceptualization: BCW, BA. Methodology: BCW, PPM, SKN, YG, AV, DJ, BA. Investigation: BCW, YY, PPM, TP, YM, FU, GK, MT, SPM, SKN, AB, HF, JJ, KK, BGW, RD, AT, SS, NG, XX. Project Administration: BCW, ZF, YG, AV, DJ, BA. Supervision: XX, ZF, YG, AV, DJ, BA. Writing – original draft: BCW, YY, TP, GK, SKN, JJ, KK. Writing – review & editing: All authors

Competing interests:

BCW and BA declare that a provisional patent on the synthesis of high-entropy MAX phases has been filed under patent number 70880-01. YG declares his role as a Board member of MXene Inc. YG is also affiliated with Sumy State University, Ukraine. All other authors declare no competing interests.

Data availability:

All data is available in the manuscript or the supplementary material.

Supplementary Materials:

Materials and Methods

Supplementary Text

Figs. S1 to S91

Tables S1 to S6

References *(47-69)*